From Molecules to the Crystalline Solid: Secondary Hydrogen-Bonding Interactions of Salt Bridges and Their Role in Magnetic Exchange

Dimitris Papoutsakis,[a] James P. Kirby,[a] James E. Jackson,*[b] and Daniel G. Nocera*[a]

Abstract: The primary two-point hydrogen-bond contact of *p*-substituted benzamidinium cations to benzoate anions in [D_6]DMSO forms a salt bridge as described by a classical Hammett relation. At carboxylate: amidinium proportions greater than 1:1, amidinium hydrogen atoms external to the salt bridge associate to carboxylate. This complementary interaction of four protons and four lone pairs of the amidinium–carboxylate salt bridge creates closure of the hydrogen-bonding network in 3-amidinium benzoate. Structural characterization of this solid shows that the primary amidinium–carboxylate interaction of the salt bridge, which leads to zigzag tapes, is augmented by lateral hydrogen bonding, forming ladder structures of oppositely oriented salt bridges. The ladders crosslink tapes, thus setting the three-dimensional structure of the system. We have exploited this secondary hydrogen-bonding interaction to construct layered magnetic solids based on the salt bridge formed between 3-cyanobenzamidinium and 2,2,4,4-tetramethylpyrroline-*N*-oxyl-3-carboxylate. In this solid, the nitroxyl radical moiety participates in the hydrogen-bonding network, truncating salt bridge ladder formation by capping (salt bridge)$_2$ ladder segments. These segments are linked to each other via the secondary hydrogen-bonding interaction of the salt bridge to form isolated linear chains of nitroxyl radicals running diagonally within the layer. Magnetic susceptibility studies show that the nitroxyl spin can propagate through the secondary hydrogen bond. When a water molecule in the solid formed from benzamidinium and 2,2,5,5-tetramethyl-3-carboxypyrroline-1-oxyl interrupts the pathway, magnetic coupling of the spins is obstructed. These results show that the hydrogen bonds external to salt bridges can both set structure and mediate magnetic organization, establishing the salt bridge as a useful synthon in the design of layered magnetic materials.

Keywords: crystal engineering · hydrogen bonds · layered compounds · magnetic properties · supramolecular salt-bridges

Introduction

The catenation of molecular subunits by hydrogen bonding to afford extended solids offers the possibility of materials design with targeted properties. When the molecular subunit carries a spin, magnetic solids may result, which differ from the isolated molecule to the extent that magnetic exchange is conveyed through the crystals' network of intermolecular bonds.[1] The construction of such solids from molecular building blocks requires that the structural subunits' noncovalent interactions, known as supramolecular synthons,[2] be controlled in a predictable manner. Of the various noncovalent intermolecular interactions that have been exploited in solids design,[3] electrostatic forces and hydrogen bonding have emerged as general tools for the assembly of molecular subunits into extended arrays. The pioneering work of Etter and Ward[4] and others[5,6] have shown that the problems associated with the nondirectionality of electrostatic interactions, the difficulty of de-solvating charged species from polar media, and the need for counterions to maintain charge neutralization in the crystalline environment are overcome when the synthon is a salt bridge. The strong primary electrostatic interaction of the salt bridge often engenders tape or layer structures. Crystallinity, however, requires order in all three dimensions, which can be particularly difficult for structures composed of tapes.[7] We now show that the secondary one-point hydrogen bonds external to amidinium–carboxylate salt bridges offer a rational mechanism for establishing three-dimensional crystalline arrays and may serve as a viable conduit for magnetic communication among the spins of paramagnetic subunits.

[a] Prof. D. G. Nocera, D. Papoutsakis
Department of Chemistry, 6–335
Massachusetts Institute of Technology
77 Massachusetts Avenue, Cambridge, MA 02139–4307 (USA)
Fax: (+1) 617-253-7670
E-mail: nocera@mit.edu

[b] Prof. J. E. Jackson, J. P. Kirby
Department of Chemistry
Michigan State University
East Lansing, Michigan 48824 (USA)
Fax: (+1) 517-353-1793
E-mail: jackson@cem.msu.edu

0947-6539/99/0505-1474 $ 17.50+.50/0

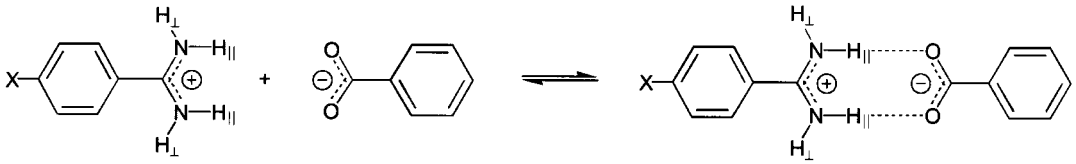

Scheme 1.

Our self-assembly scheme centers on the primary two-point hydrogen bond of the amidinium–carboxylate salt bridge (Scheme 1) augmented by secondary hydrogen bonds between the external amidinium hydrogens and carboxylate oxygens of neighboring salt bridges. In this work, we provide evidence for the secondary interaction in solution and show that it sets the connectivity for the design of a three-dimensional layered solid based on 3-amidinium benzoate. The structure exploits the propensity of the salt bridge to form a closed set of hydrogen bonds thus providing the link between molecules in solution and the crystalline solid state. Spin is introduced into the layered solid by isolating the amidinium and carboxylate functionalities on separate molecular subunits, with the carboxylate bearing the paramagnetic nitroxide 2,2,5,5-tetramethyl-3-carboxypyrroline-1-oxyl. Salts of this anion with 3-cyanobenzamidinium preserve the primary two-point and secondary one-point interactions while the nitroxyl group assumes a dual role as a spin carrier and as a crystal engineering element. We show that spins may magnetically couple through the secondary amidinium-carboxylate hydrogen bonds, establishing this salt-bridge as a supramolecular synthon in the assembly of molecular magnetic materials.

Experimental Section

Materials: The carboxylate of the previously known 3-amidinium chloride benzoic acid,[8] 3-amidinium benzoate (**1**), was prepared in a one-pot synthesis from the corresponding 3-cyanobenzoic acid by base-catalyzed ammonolysis of the nitrile, as we have previously described.[9] An excess of freshly generated sodium methoxide in a methanol solution of 3-cyanobenzoic acid, under an argon atmosphere, performed the dual duties of deprotonating the acid to yield the benzoate and converting the nitrile to the free base imidate ester carboxylate. Addition of excess ammonium chloride after 24 h of stirring, at ambient temperature, yields **1**, which was filtered and washed several times with water, methanol and ether and recrystallized from hot water. ^{1}H NMR (300 MHz, D_2O, TMS): $\delta = 7.67$ (1H, t), 7.89 (1H, d), 8.18 (1H, d), 8.20 (1H, s). Elemental analysis was performed by H. Kolbe Mikroanalytisches Laboratorium. $C_8H_8N_2O_2$ (%): calcd: C 58.53, H 4.91, N 17.06; found: C 58.36, H 4.99, N 16.89.

3-Cyanobenzamidinium chloride was synthesized in a similar manner. 1,3-dicyanobenzene (5.125 g, 40 mmol) was placed under an argon atmosphere in a flame-dried Schlenk flask, equipped with a magnetic stirrer. A freshly generated solution of sodium methoxide in methanol (0.46 g, 20 mmol, of Na in 100 mL of methanol) was added dropwise at ambient temperature. The solid was dissolved within 30 min, and the clear solution was stirred at room temperature for an additional 2 h. Ammonium chloride (5.35 g, 100 mmol) was added and stirring continued overnight. The solvent was removed under vacuum and the white solid was heated at 80 °C under vacuum for an additional 3 h. It was washed with ether and methanol and recrystallized from water producing fine white needles, which were air dried for 24 h. ^{1}H NMR (300 MHz, [D_6]DMSO): $\delta = 7.80$ (1H, t, J = 9 Hz), 8.16 (2H, t, J = 9 Hz), 8.34 (1H, s), 9.57 (4H, s).

The salts 3-cyanobenzamidinium-2,2,5,5-tetramethyl-3-carboxypyrroline-1-oxyl (**2**) and benzamidinium-2,2,5,5-tetramethyl-3-carboxypyrroline-1-oxyl (**3**) were prepared by slow evaporation of aqueous solutions containing equimolar amounts of the corresponding amidinium chloride and the 2,2,5,5-tetramethyl-3-carboxypyrroline-1-oxyl neutralized by 1,8-diazabicyclo[5.4.0]undec-7-ene (DBU). The resulting yellow crystals of **2** and **3** were removed from their mother liquors prior to complete evaporation of the water. The results of elemental analyses, also performed by H. Kolbe Mikroanalytisches Laboratorium are as follows: **2**: $C_{17}H_{21}N_4O_3$ (%): calcd: C 61.99, H 6.43, N 17.00; found: C 62.11, H 6.49; N 17.10; **3**: $C_{16}H_{24}N_3O_4$ (%): calcd: C 59.61, H 7.50, N 13.03; found: C 59.60, H 7.48, N 13.12.

Methods: Solid-state infrared spectra were recorded as KBr pellets on a Perkin Elmer Spectrum 2000 spectrophotometer with a resolution of 1 cm^{-1}. Prominent absorptions were observed at 3270, 3170, and 3253 cm^{-1} for **1**, **2**, and **3** respectively. EPR spectra were recorded at room temperature by using an X-band Bruker ESP300E spectrometer. Solution samples were prepared by dissolving the solid materials in deuterated methanol at a concentration of 10^{-4} M, followed by thorough deoxygenation afforded from several freeze-thaw cycles under vacuum. The spectrum in Figure 7b was recorded with a magnetic field modulation of 0.04 G, microwave power of 1 mW and field modulation frequency of 25 kHz to avoid any possible complication from modulation sidebands.[10] Simulations were performed by using Bruker's program SimFonia. Magnetic susceptibilities were determined using a SQUID susceptometer (Quantum Design MPMSR2 Susceptometer) within the 2 to 300 K temperature range. The data were corrected for the diamagnetic contribution of the sample holder and for the diamagnetism of the compound, calculated using Pascal's constants. To ensure that powder samples were consistent with the results of X-ray crystallography, the powder X-ray diffraction pattern was calculated from the atomic coordinates and cell dimensions of the X-ray crystal data (see below). Calculated and observed powder X-ray diffraction patterns of the compounds were in excellent agreement with each other.

A Varian Gemini-300 spectrometer was used to record the ^{1}H NMR spectra of *p*-substituted benzamidinium-benzoates in [D_6]DMSO. The chemical shifts were referenced to the residual solvent peaks. The association constants were determined from the chemical shifts of the ^{1}H NMR of the $NH_{\parallel}$ for freely solvated amidinium (δ_{am}) and for the amidinium carboxylate salt bridge ($\delta_{am\text{-}ca}$). The difference in these chemical shifts, $\Delta\delta_{max}$ ($= \delta_{am\text{-}ca} - \delta_{am}$) is related to the observed carboxylate concentration-dependent chemical shift, δ_{obs}, according to expression (1). The association constant for the salt bridge is obtained from a nonlinear least-squares fit of the data to this relation.

$$\delta_{obs} = \delta_{Am} + \frac{\Delta\delta_{max}}{2[Am]_0}\left[\frac{1}{K_{assoc}} + [Am]_0 + [Ca]_0 - \sqrt{\left(\frac{1}{K_{assoc}} + [Am]_0 + [Ca]_0\right)^2 - 4[Am]_0[Ca]_0}\right] \quad (1)$$

Experimental details of the X-ray analyses of the salts presented here are given in Table 1. Single-crystal X-ray data were collected on a Rigaku diffractometer with graphite-monochromated $Mo_{K\alpha}$ radiation ($\lambda = 0.71073$ Å) to a maximum of $2\theta = 50°$. Final cell parameters were obtained by least-squares analyses of 22–24 reflections, while all data were corrected for Lorentz and polarization effects. Absorption correction was based on ψ scans of a few suitable reflections with χ values close to 90°. The structures were solved by using direct methods (SHELXS-86) and refined by using full-matrix least-squares procedures based on F^2 (SHELXL-93). All non-hydrogen atoms were refined anisotropically. Amidinium hydrogen atoms were located after successive Fourier difference maps and refined isotropically, while all other hydrogen atoms were placed in idealized positions with assigned isotropic temperature factors ($U = 1.2U$ of bonded atoms).[11]

Table 1. Crystallographic data for compounds **1**–**3**.

	1	**2**	**3**
		Crystal parameters	
formula	$C_8H_8N_2O_2$	$C_{17}H_{21}N_4O_3$	$C_{16}H_{24}N_3O_4$
FW	164.16	329.38	322.38
crystal size [mm^3]	$0.65 \times 0.40 \times 0.20$	$0.46 \times 0.23 \times 0.15$	$0.57 \times 0.32 \times 0.30$
crystal system	monoclinic	monoclinic	monoclinic
space group	$P2_1/n$	$P2_1/c$	$P2_1/n$
a [Å]	7.253(2)	8.107(4)	9.232(1)
b [Å]	6.934(3)	18.463(2)	9.479(5)
c [Å]	14.602(2)	12.231(2)	20.695(3)
β [°]	93.64(2)	103.15(2)	97.94(2)
V [Å^3]	733.0(4)	1782.9(9)	1793.8(9)
Z	4	4	4
ρ_{calcd} [g cm^{-3}]	1.488	1.227	1.194
$F(000)$	344	700	692
$\mu(Mo_{K\alpha})$ [cm^{-1}]	1.10	0.86	0.86
		Data collection	
$2\theta_{max}$ [°]	50.0	50.0	50.0
index ranges	$0 \le h \le 8$	$0 \le h \le 9$	$0 \le h \le 9$
	$0 \le k \le 8$	$0 \le k \le 21$	$0 \le k \le 11$
	$-17 \le l \le 17$	$-14 \le l \le 14$	$-24 \le l \le 24$
scan speed [° min^{-1} in ω]	2	2	2
T [K]	296(2)	296(2)	296(2)
reflections collected	1397	3369	2937
unique reflections	1288	3140	2725
R(merg) [%]	3.27	2.99	4.53
		Refinement	
refinement method	full-matrix least-squares on F^2	full-matrix least-squares on F^2	full-matrix least-squares on F^2
R indices ($I > 2\sigma(I)$)	$R1 = 0.0376$	$R1 = 0.0522$	$R1 = 0.0459$
	$WR2 = 0.1195$	$WR2 = 0.1054$	$WR2 = 0.1090$
R indices all data	$R1 = 0.0519$	$R1 = 0.1275$	$R1 = 0.0918$
	$WR2 = 0.1291$	$WR2 = 0.1370$	$WR2 = 0.1334$
$\Delta(\rho)$ [e Å^{-3}]	0.180	0.177	0.152
extinction coefficient	0.034(9)	0.005(1)	0.016(2)
GOF	1.174	1.030	1.135

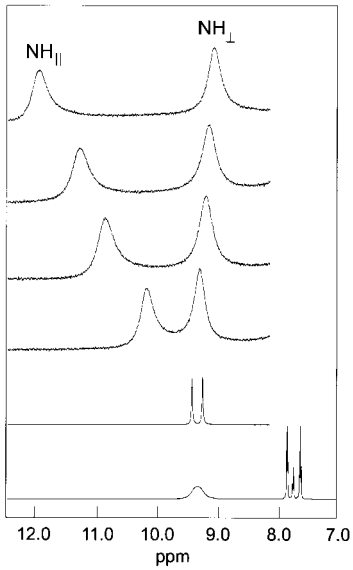

Figure 1. Selected ^{1}H NMR spectra of the equilibrium described in Scheme 1 for X = H (5.2 mM in [D$_6$]DMSO) in the absence of tetrabutylammonium benzoate with no benzoic acid, with the addition of a catalytic amount of benzoic acid and subsequent additions of 1.5, 2.3, 3.0, and 5.0 mM tetrabutylammonium benzoate (bottom to top). The spectral range captures the amidinium protons internal (NH$_\parallel$) and external (NH$_\perp$) to the salt bridge interface; the initial spectrum also shows the ^{1}H spectral region of the phenyl rings.

Results and Discussion

More than 100 years ago Pinner isolated benzamidinium–benzoate salts in his pursuit of a synthetic methodology toward the amidinium functional group.[12] In solution, amidinium spontaneously interacts with a carboxylate to form a salt bridge as depicted in Scheme 1 for benzamidinium–benzoate. The interfacial protons (NH$_\parallel$) *anti* to the aryl group mediate this two-point interaction, leaving the other pair (NH$_\perp$) for additional one-point contacts. We have studied this equilibrium where X is hydrogen, methyl, phenyl, or trifluoromethyl. In the presence of added benzoic acid (16.6 mM),[13] the NH$_\parallel$ and NH$_\perp$ resonances appear as two resolvable peaks centered at $\delta = 9.3$ ppm. Figure 1 shows the ^{1}H NMR spectral changes resulting from the addition of varying amounts of tetrabutylammonium benzoate to benzamidinium chloride in [D$_6$]DMSO. A concentration-dependent downfield shift of amidinium protons involved in hydrogen bonding (NH$_\parallel$ varying by >3 ppm) to carboxylate is contrasted by an insensitivity of the chemical shift (<0.5 ppm) for the amidinium protons external to the salt bridge (NH$_\perp$). Such behavior, which has been observed previously for bicyclic guanidinium–carboxylate[14] and amidinium–phosphate complexation,[15] is a signature of salt bridge formation. A nonlinear least-squares fit[16] of chemical shift of the hydrogen-bonded amidinium protons versus the carboxylate concentration yields an association constant (K_{assoc}) of 2500 M^{-1} in [D$_6$]DMSO. A 1:1 stoichiometry for the complex over a 0–25 mM concentration range of benzoate (benzamidinium concentration of 5.5 mM) is established by a Job's plot[17] of the ^{1}H NMR titration data, which shows that the complex is optimally formed at equimolar concentrations of amidinium and carboxylate (i.e., a 0.5 mole fraction). Two favorable secondary electrostatic interactions (SEI),[18] composing the hydrogen-bonded interface contribute to the exceptionally high association of the salt bridge in a solvent of such large dielectric constant as [D$_6$]DMSO. However SEI cannot entirely account for the stability of the salt bridge inasmuch as the structurally analogous two-point hydrogen bonds between urea and carboxylate,[19] which also exhibit a SEI of 2, yield association constants that are more than a factor of 10 less than that observed here. In our case, the charge–dipole interaction of the SEI is subsumed in the simple charge–charge electrostatic attraction between the negative carboxylate and positive amidinium ions.

The strength of the salt bridge described by Scheme 1 directly correlates with the electronic properties of the individual constituents. Figure 2 displays a plot of the log of K_{assoc} (as referenced to X = H) versus the Hammett σ_p parameter.[20] The linear free energy relation (slope $\rho = 1.4$) of Figure 2, which is characteristic of benzamidinium–benzoate[21] and other primary two-point hydrogen bond systems,[22,23] indicates that association is governed by the acidity of the amidinium partner as dictated by the composite resonance and sigmatropic electron-withdrawing/electron-donating effects of X in the para position on the phenyl ring.

0947-6539/99/0505-1476 $ 17.50+.50/0 *Chem. Eur. J.* **1999**, *5*, No. 5

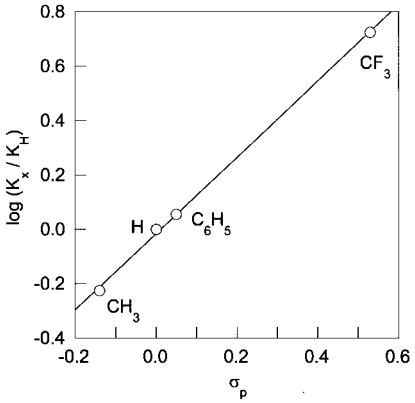

Figure 2. Plot of the K_{assoc} for the equilibrium represented in Scheme 1 (normalized to K_{assoc} for X = H) vs Hammett σ_p parameter (slope, $\rho = 1.4$).

As the concentrations of amidinium and benzoate partners are increased beyond 25 mM, new equilibria are observed in addition to the one associated with the primary two-point hydrogen bond. Specifically, whereas the chemical shift of the $NH_{\parallel}$ protons becomes nearly independent of benzoate at high concentrations (owing to saturation equilibrium of the axial hydrogens), the $NH_{\perp}$ protons exhibit a pronounced downfield chemical shift. This behavior, displayed in Figure 3 over a carboxylate concentration range of 0 to 864 mM,

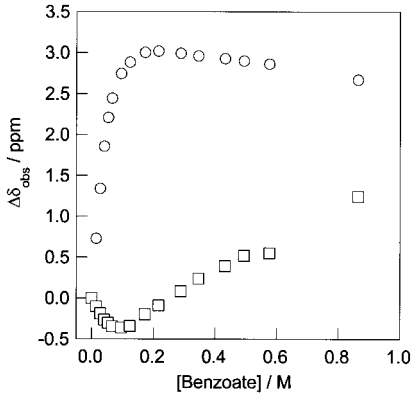

Figure 3. The change in the chemical shift of $NH_{\parallel}$ (circles) and $NH_{\perp}$ (squares) with the addition of benzoate (0 to 864 mM) in the presence of 226 mM benzoic acid (see ref. [13]). The concentration of benzamidinium was 63 mM.

suggests the presence of a secondary equilibrium involving hydrogen bonding to $NH_{\perp}$. As formalized by graph set analysis,[24] one primary two-point $NH_{\parallel}$ and two secondary one-point NH hydrogen bonds lead to a closed set of hydrogen bonds for the salt bridge. As we now show, this connectivity forms the architectural underpinning for layered crystalline solids constructed from amidinium–carboxylate salt bridges.

In order to elaborate an extended structure, the amidinium and carboxylate functionalities were introduced at the 1 and the 3 positions of the same phenyl ring. Figure 4 (top) shows the *bc* plane of the crystal structure of 3-amidinium benzoate (**1**). Typical of a 1,3-phenyl substitution pattern, a two-dimensional zigzag tape structure forms from the catenation of the two-point hydrogen bonds along a chain. Tapes align in

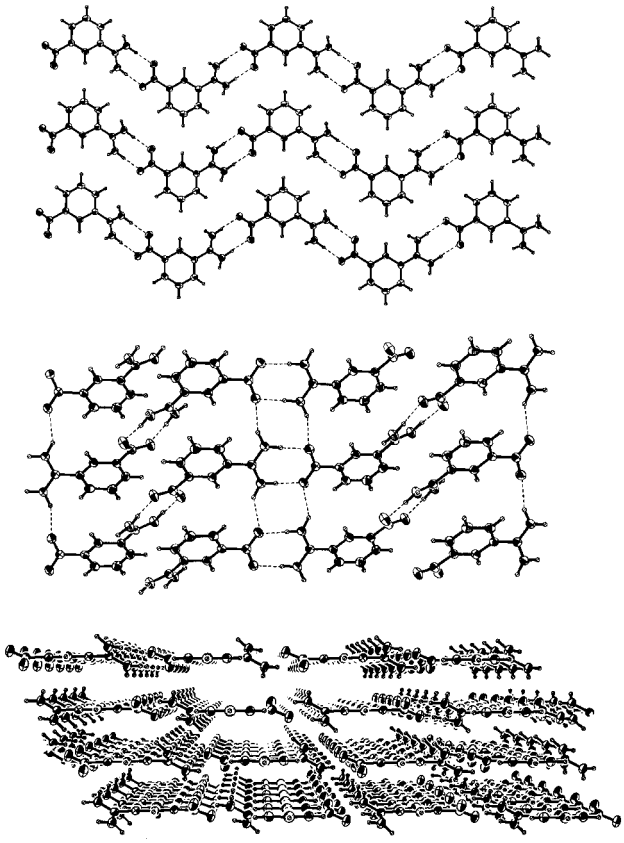

Figure 4. The packing of the zigzag tapes in the *bc* plane of the crystal structure of **1** (top). Rotation of the crystal structure of **1** such that the ladder is viewed in the plane of the paper (middle). The *ac* plane of the crystal structure of **1** showing the layered sheet structure supported by the ladder scaffold. The ladders tilt alternately in to and out of the plane of the paper by 30.0° and 23.3°, respectively (bottom).

a head-to-head arrangement along the *c* axis of the unit cell and pack together at a van der Waals contact distance to create the sheets of the *bc* plane. The repeat distance between positional atoms of neighboring tapes is 6.93 Å thereby establishing the *b* dimension of the unit cell. Whereas the phenyl rings lie in the *bc* plane, a rotation of the amidinium group by 30.0(1)° from the plane of the aromatic ring is complemented by a 23.3(1)° counter-rotation of the carboxylate group. This 7° difference in rotation of the two groups results in a slight twist of the amidinium–carboxylate interface (dihedral angle of 8.41° for the planes defined by the CN_2 and CO_2 atoms of the salt bridge) with respect to the *bc* plane. Nonetheless, the interface is very stable as indicated by the relatively short N–O distances of 2.766(1) Å (∢NHO 177(2)°) and 2.791(2) Å (∢NHO 180(2)°) and by the self-assembly of the salt bridge from aqueous solution.

The canting of the salt bridges permits the formation of secondary hydrogen-bonding interactions akin to that observed in solution, thus extending the dimensionality of the structure beyond the sheets of zigzag tapes. The amidinium protons outside the salt bridge ($H_{\perp}$) form hydrogen bonds to carboxylate oxygens of tapes from adjacent sheets above and below the *bc* plane. Consistent with solution results, the one-point hydrogen bond is slightly weaker than the two-point interaction, as evidenced by longer N–O distances of

2.878(2) Å (∢NHO 153(2)°) and 2.905(2) Å (∢NHO 143(2)°). As shown in Figure 4 (middle), this secondary interaction generates ladders, which radiate from the aromatic subunits to provide the scaffolding to support a layer structure of interconnecting sheets of zigzag tapes (Figure 4 bottom). The structure is further stabilized by the van der Waals interactions of the aromatic rings from neighboring sheets (*d* spacing 3.16 Å). The hydrogen-bonding arrangement of the ladder necessarily enforces the amidinium–carboxylate salt bridges in neighboring sheets to arrange with their dipoles opposed, thereby setting the head-to-tail orientation of tapes along the ladder. This head-to-tail orientation has the added benefit of satisfying the dominant Coulomb interaction within the three-dimensional structure since dipoles of salt bridges along the ladder are at a distance of 3 Å whereas the dipoles of salt bridges within the *bc* plane are at a distance of 7 Å.

The same interactions of the four protons and four lone pairs of the amidinium–carboxylate salt bridge that we observe in solution creates closure of the hydrogen-bonding network in **1**. Two protons internal ($H_{\parallel}$) to the salt bridge establish a primary interaction with two lone pairs of a carboxylate; the resulting zigzag tapes are like those of isophthalic acid,[25] where carboxylic acid dimers form the two-point intermolecular hydrogen bonds. However, in isophthalic acid, there is no secondary interaction to connect the layers owing to the absence of protons external to the hydrogen-bonding interface. For the amidinium–carboxylate salt bridge of **1**, the two external protons of the salt bridge ($H_{\perp}$) are complemented by two lone pairs on oxygens from adjacent interlayer carboxylates to form the common ladder structure characteristic of benzamidinium–carboxylate bridges.[26] In accordance with the recent predictions of Whitesides,[7] a secondary interaction external to the tape is the critical structural element that establishes the three-dimensional motif of the crystal.

Whereas **1** is not able to support an unpaired electron, the introduction of the carboxylate and amidinium moieties in separate species permits spin to be introduced into an engineered layered structure. In compound **2**, the nitroxyl carboxylate 2,2,5,5-tetramethyl-3-carboxypyrroline-1-oxyl complexes with 3-cyanobenzamidinium to form a layered structure with amidinium-carboxylate linkages similar to those in **1**. Figure 5 displays the amidinium–carboxylate salt bridge of **2**, which is somewhat unsymmetrical with its N–O distances of 2.853(3) Å (∢NHO 166(3)°) and 2.680(3) Å (∢NHO 172(3)°). Both functionalities within the salt bridge interface are twisted with respect to the planes defined by the ring backbones of their constituent molecular units. As in **1**, rotations of the carboxylate and amidinium groups (by 20.8(3)° and 34.7(3)°, respectively) set up the amidinium–carboxylate ladder structure through the one-point carboxylate-O to $H_{\perp}$ contacts, with d(N–O) = 2.789(4) Å (∢NHO 155(3)°). Ladder formation is truncated at four-molecule segments by hydrogen-bonding of the external amidinium $H_{\perp}$ protons to the nitroxyl oxygens of adjacent ladder segments. Closure of the hydrogen-bonding network through this nitroxyl-to-ladder interaction (d(N–O) 2.851(3) Å (∢NHO 178(3)°)) engenders a two-dimensional network, as shown in Figure 6, thus extending the dimensionality of the solid. The aromatic units of the cation, which are positioned in a face to face arrangement, occupy the intralayer volume. The cyano group is not involved in any close contacts and adjacent layers simply stack on top of each other.

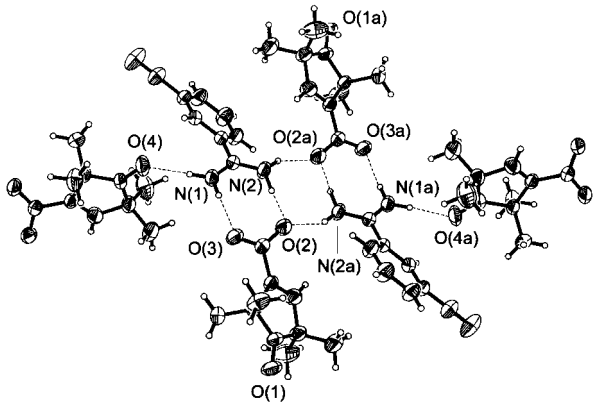

Figure 5. Crystal structure of 3-cyanobenzamidinium-2,2,5,5-tetramethyl-3-carboxypyrroline-1-oxyl (**2**) highlighting the four molecule amidinium–carboxylate cluster, hydrogen bonded to two nitroxyl radicals external to the ladder subunit.

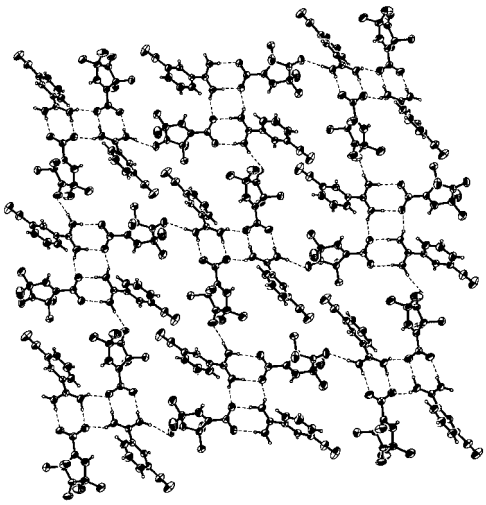

Figure 6. Two-dimensional sheets of compound **2** assembled by nitroxyl radicals interconnecting adjacent cluster subunits. The nitroxyl spin carriers compose a linear chain, diagonally situated within the layer.

The solution EPR spectrum of compound **2** shown in Figure 7a displays the typical three-line pattern, with the splitting arising from the ^{14}N hyperfine coupling to the free electron. The Landé *g* factor is 2.010 and the value of the nitrogen isotropic hyperfine coupling, obtained directly from the experimental spectrum, is 15.3 G, typical of the nitroxyl radical in solution.[27] As has been noted previously,[28] oxygen-free solutions of nitroxyl compounds provide additional details regarding proton superhyperfine (shf) coupling. Figure 7b displays the central nitrogen hyperfine line of compound **2**, where good resolution of the proton hyperfine is observed. Computer simulation of the spectrum yields values of 0.235 G and 0.465 G for the coupling to the methyl and vinylic protons respectively, in agreement with literature results.[27b,c] These

0947-6539/99/0505-1478 $ 17.50+.50/0 *Chem. Eur. J.* **1999**, *5*, No. 5

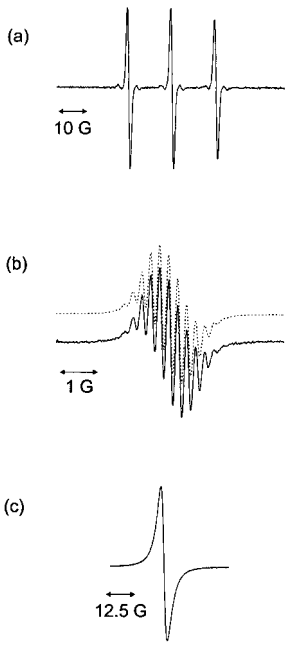

Figure 7. Room temperature ESR spectra of compound **2** (a) in deuterated methanol, (b) in deoxygenated deuterated methanol, and (c) for a solid sample.

values establish that delocalization of the unpaired electron is not limited to the nitroxyl moiety, but extends to the ring backbone of the radical.

Powder EPR experiments afforded featureless, relatively broad gaussian-shaped line profiles (Figure 7c). The lack of hyperfine splitting in the solid yields no information regarding exchange interactions. Consequently, magnetic susceptibility measurements on powder specimens were undertaken. Figure 8 illustrates the $\chi_M T$ vs T plot. Negative deviation from the high-temperature spin-only value of 0.360 and a Weiss constant of -1.1 K indicates antiferromagnetic coupling between the nitroxyl spins.

Examination of Figures 5 and 6 reveals four possible pathways for spin communication, all of which involve the salt bridge. Taking the nitroxyl oxygen as the seat of unpaired spin, and tracing paths in the six-subunit fragment shown in Figure 5, we designate O(1)···O(4), O(1)···O(4a), O(4)···O(4a), and O(1)···O(1a) as paths 1–4, respectively. The first, and shortest, is the one we believe to be magnetically significant (see below); it is a nine-bond path in which nitroxyl radicals internal and external to the four molecule ladder cluster are coupled through N–O(4)···$H_\perp$–N(1)–$H_\parallel$···O(3)–C hydrogen bonding. Paths 2, 3, and 4 involve 11, 12, and 14 bonds, respectively; path 3, propagating along and across the ladder cluster, includes four hydrogen bonds rather than the two found in each of the other three paths. It is unlikely that the transfer of spin through paths 2–4 could effectively compete with the shorter path 1. As can be seen in Figure 6, path 1 composes isolated linear chains of nitroxyl radicals running diagonally within the layer. On this basis, we have analyzed the magnetic susceptibility data of **2**, shown in Figure 8, using a Heisenberg linear chain model.[29] By using the experimentally determined Landé g factor, we obtain $J/k_B = -0.8$ K.

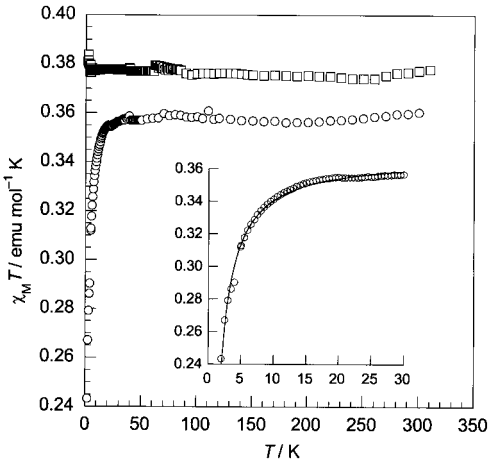

Figure 8. Temperature dependence of the magnetic susceptibility of **2** (○) and **3** (□). The inset shows the least-squares fit over the temperature range of greatest change of the magnetic susceptibility data of **2** to a Heisenberg linear chain model.

We probed the effectiveness of the spin propagation along the chain by examining compound **3**, shown in Figure 9. Here, the 3-cyanobenzamidinium of **2** has been replaced with unsubstituted benzamidinium. The same four-cluster unit is

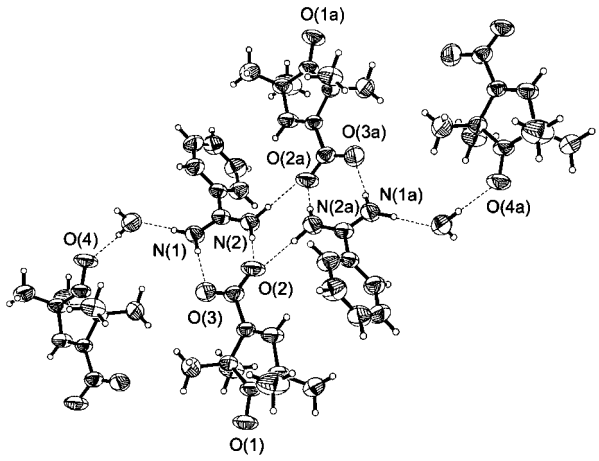

Figure 9. Crystal structure of benzamidinium-2,2,5,5-tetramethyl-3-carboxypyrroline-1-oxyl (**3**) highlighting the four molecule amidinium–carboxylate cluster, hydrogen-bonded to two nitroxyl radicals external to the ladder structure through two water molecules.

retained with nearly identical metrical parameters, but a water molecule interrupts the hydrogen bond connecting the internal and external nitroxyl radicals. As Figure 8 reveals, the $\chi_M T$ vs T plot renders a straight line of slope = 0 and intercept of 0.377 for $T = 2-300$ K, indicating purely paramagnetic behavior.

The differing magnetic behavior of **2** and **3** suggests that coupling between external and internal nitroxyl radicals is the important exchange pathway since it is the presence or absence of this interaction that distinguishes these structures.[30] If intracluster coupling were dominant, then similar behavior for both compounds would be expected on the basis of the retention of path 4 in both structures. Moreover, these data support our initial inference that path 1 should dominate the magnetic coupling; the extra H_2O in **3** adds one hydrogen bond and one O–H covalent bond to path 1, making it an 11-bond pathway that includes three hydrogen bonds. Noting that path 2 is an 11-bond linkage incorporating two hydrogen bonds, and that path 3 has 14 bonds with four hydrogen bonds, it seems unlikely that these connections contribute to the coupling in **2**.

The most successful approaches to crystal engineering take advantage of the highly directional and relatively strong nature of the hydrogen bond. The secondary hydrogen bond of a salt bridge is strong with respect to other noncovalent secondary interactions and is important in setting the dimensionality of layered structures. This structural element

is also capable of propagating magnetism within the layer when radical centers are introduced. Although the spin is mainly localized on the molecular constituents composing the layer, small but appreciable amounts of spin density can advance through the intermolecular hydrogen bonds external to the salt bridge as observed for spin polarization mechanisms of other hydrogen bonds.[1,31–34] These results show that the hydrogen bonds external to salt bridges can both set structure and mediate magnetic organization, establishing the salt bridge as a useful synthon in the design of layered magnetic materials.

[1] M. M. Matsushita, A. Izuoka, T. Sugawara, T. Kobayashi, N. Wada, N. Takeda, M Ishikawa, *J. Am. Chem. Soc.* **1997**, *119*, 4369.

[2] G. R. Desiraju, *Angew. Chem.* **1995**, *107*, 2541; *Angew. Chem. Int. Ed. Engl.* **1995**, *34*, 2311.

[3] a) G. M. Whitesides, J. P. Mathias, C. T. Seto, *Science* **1991**, *254*, 1312; b) J. C. MacDonald, G. M. Whitesides, *Chem. Rev.* **1994**, *94*, 2383.

[4] a) V. A. Russell, M. C. Etter, M. D. Ward, *J. Am. Chem. Soc.* **1994**, *116*, 1941; b) V. A. Russell, M. C. Etter, M. D. Ward, *Chem. Mater.* **1994**, *6*, 1206; c) V. A. Russell, M. D. Ward, *Chem. Mater.* **1996**, *8*, 1654; d) J. A. Swift, V. A. Russell, M. D. Ward, *Adv. Mater*. **1997**, *9*, 1183; e) V. A. Russell, C. C. Evans, W. J. Li, M. D. Ward, *Science*, **1997**, *276*, 575.

[5] M. W. Hosseini, R. Ruppert, P. Schaeffer, A. De C. Cian, N. Kyrisakas, J. Fischer, *J. Chem. Soc. Chem. Commun.* **1994**, 2135.

[6] a) C. B. Aakeröy, P. B. Hitchcock, B. D. Moyle, K. R. Seddon, *J. Chem. Soc. Chem. Commun.* **1992**, 553; b) C. B. Aakeröy, M. Nieuwenhuyzen, *J. Am. Chem. Soc.* **1994**, *116*, 1098; c) C. B. Aakeröy, D. P. Hughes, M. Nieuwenhuyzen, *J. Am. Chem. Soc.* **1996**, *118*, 10134; d) C. B. Aakeröy, *Acta Crystallogr. Sect. B* **1997**, *53*, 569.

[7] a) K. E. Schwiebert, D. N. Chin, J. C. MacDonald, G. M. Whitesides, *J. Am. Chem. Soc.* **1996**, *118*, 4018; b) S. Palacin, D. N. Chin, E. E. Simanek, J. C. MacDonald, G. M. Whitesides, M. T. McBride, G. T. R. Palmore, *J. Am. Chem. Soc.* **1997**, *119*, 11807.

[8] G. Wagner, H. Vieweg, H. Kuehmstedt, *Pharmazie* **1973**, *28*, 288.

[9] a) J. P. Kirby, N. A. van Dantzig, C. K. Chang, D. G. Nocera, *Tetrahedron Lett.* **1995**, *36*, 3477; b) J. P. Kirby, J. A. Roberts, D. G. Nocera, *J. Am. Chem. Soc.* **1997**, *118*, 9230; c) J. A. Roberts, J. P. Kirby, S. T. Wall, D. G. Nocera, *Inorg. Chim. Acta.* **1997**, *263*, 395.

[10] J. S. Hyde, H. W. Brown, *J. Chem. Phys.* **1962**, *37*, 368.

[11] Crystallographic data (excluding structure factors) for the structures reported in this paper have been deposited with the Cambridge Crystallographic Data Centre as supplementary publication no. CCDC-101012 (**1**), CCDC-101576 (**2**), and CCDC-101575 (**3**). Copies of the data can be obtained free of charge on application to CCDC, 12 Union Road, Cambridge CB21EZ, UK (fax: (+44) 1223-336-033; e-mail: deposit@chemcrys.cam.ac.uk).

[12] A. Pinner, *Die Imidoäther und ihre Derivate*, Oppenheim, Berlin, **1892**.

[13] Benzoic acid catalyzes the exchange of amidinium protons thereby rendering them observable by circumventing inhomogeneous line broadening. The association of benzoic acid to benzamidinium is negligible (B. Kratochvíl, J. Ondrácek, J. Hasek, L. Csordás, *Collect. Czech. Chem. Commun.* **1988**, *53*, 3131).

[14] G. Müller, J. Riede, P. Schmidtchen, *Angew. Chem*. **1988**, *100*, 1574; *Angew. Chem. Int. Ed. Engl.* **1988**, *27*, 1516.

[15] M. W. Göbel, J. W. Bats, G. Dürner, *Angew. Chem*. **1992**, *104*, 217; *Angew. Chem. Int. Ed. Engl.* **1992**, *31*, 207.

[16] C. S. Wilcox in *Frontiers in Supramolecular Organic Chemistry and Photochemistry*, (Eds.: H.-J. Schneider, H. Durr) VCH, Weinheim, **1991**, p. 123.

[17] K. A. Connors, *Binding Constants: A Measure of Molecular Complexation and Stability*, Wiley, New York, **1987**.

[18] a) J. Pranata, S. G. Wierschke, W. L. Jorgensen, *J. Am. Chem. Soc.* **1991**, *113*, 2810; b) W. L. Jorgensen, J. Pranata, *J. Am. Chem. Soc.* **1990**, *112*, 2008.

[19] T. R. Kelly, M. H. Kim, *J. Am. Chem. Soc.* **1994**, *116*, 7072.

[20] D. C. Johnson, *The Hammett Equation*, Cambridge University Press, Cambridge, **1973**.

[21] a) J. Krechl, S. Smrckova, J. Kuthan, *Collect. Czech. Chem. Commun.* **1990**, *55*, 460. b) J. Krechl, S. Smrckova, F. Pavlikova and J. Kuthan, *Collect. Czech. Chem. Commun.* **1989**, *54*, 2415.

[22] K. A. Haushalter, J. Lau, J. D. Roberts, *J. Am. Chem. Soc.* **1997**, *118*, 8891.

[23] C. S. Wilcox, E. Kim, D. Romano, L. H. Kuo, A. L. Burt, D. P. Curran, *Tetrahedron* **1995**, *51*, 621.

[24] M. C. Etter, *Acc. Chem. Res.* **1990**, *23*, 120.

[25] J. L. Derissen, *Acta Crystallogr. Sect. B* **1974**, *30*, 2764.

[26] a) B. Kratochvíl, J. Ondrácek, K. Malý, L. Csordás, *Collect. Czech. Chem. Commun.* **1988**, *53*, 294; b) B. Kratochvíl, J. Ondrácek, J. Krechl, J. Hasek, *Acta Crystallogr. Sect. C* **1987**, *43*, 2182.

[27] a) A. T. Bullock, C. B. Howard, *J. Chem. Soc. Faraday I* **1980**, *76*, 1296; b) M. F. Ottaviani, G. Martini, L. Nuti, *Magn. Reson. Chem.* **1987**, *25*, 897; c) D. Mustafi, H. Joela, *J. Phys. Chem.* **1995**, *99*, 11370.

[28] a) C. A. Popp, J. S. Hyde, *J. Magn. Reson.* **1981**, *43*, 249; b) J. S. Hyde, W. K. Subczynski, *J. Magn. Reson.* **1984**, *56*, 125.

[29] Paths 1 and 2 compose linear chains, while 3 and 4 represent localized dimer interactions. Thus, in principle, the paths could be distinguished on the basis of their magnetic behavior (Heisenberg chain versus Bleaney–Bowers dimer models of the magnetic susceptibility data). However, for systems as weakly coupled as **2**, the two models' least-squares fits to the susceptibility data are so similar that no reliable distinction can be drawn on this basis. As a matter of interest, the corresponding J/k_B values are -0.8 and -1.2 K, respectively.

[30] Given the weakness of the magnetic couplings observed and the relatively long connection paths we invoke in these systems, we cannot rule out the possibility that simple through-space interactions could play a role in magnetic coupling. However, having carefully inspected the structures and packing diagrams for obvious π stacking or other close approaches, we have not found contacts more promising than these hydrogen-bonding pathways as explanations for the difference in magnetic behaviors seen between **2** and **3**. Indeed, the shortest through-space coupling distance between nitroxyl spins in paramagnetic material **3** is 6.71 Å whereas the corresponding shortest distance in the coupled antiferromagnetic system **2** is 7.28 Å. These results strongly point toward a through-bond pathway. We thus prefer the interpretation of the hydrogen bond networks because of their self-consistency with the structural chemistry.

[31] B. N. Figgis, E. S. Kucharski, M. Vrtis, *J. Am. Chem. Soc.* **1993**, *115*, 176.

[32] a) C. Kollmar, O. Kahn, *Acc. Chem. Res.* **1993**, *26*, 259; b) A. Lang, Y. Pei, L. Quahab, O. Kahn, *Adv. Mater.* **1996**, *8*, 60.

[33] a) E. Hernández, M. Mas, E. Molins, C. Rovira, J. Veciana, *Angew. Chem.* **1993**, *105*, 919; *Angew. Chem. Int. Ed. Engl.* **1993**, *32*, 882; b) J. Cirujeda, L. E. Ochando, J. M. Amigó, C. Rovira, J. Rius, J. Veciana, *Angew. Chem.* **1995**, *107*, 99; *Angew. Chem. Int. Ed. Engl.* **1995**, *34*, 55; c) J. Cirujeda, M. Mas, E. Molins, F. L. de Panthou, J. Laugier, J. G. Park, C. Paulsen, P. Rey, C. Rovira, J. M. Amigó, J. Veciana, *J. Chem. Soc. Chem. Commun.* **1995**, 709; d) J. Veciana, J. Cirujeda, C. Rovira, J. Vidal-Gancedo, *Adv. Mater.* **1995**, *7*, 221. e) C. Rovira, J. Veciana, E. Ribera, J. Tarres, E. Canadell, R. Rousseau, M. Mas, E. Molins, M. Almeida, R. T. Henriques, J. Morgado, J. P. Schoeffel, J. P. Pouget, *Angew. Chem.* **1997**, *109*, 2417; *Angew. Chem. Int. Ed. Engl.* **1997**, *36*, 2324; e) O. Jurgens, J. Cirujeda, M. Mas, I. Mata, A. Cabrero, J. VidalGancedo, C. Rovira, E. Molins, J. Veciana, *J. Mater. Chem.* **1997**, *7*, 1723.

[34] a) M. Tamura, Y. Nakazawa, D. Shiomi, K. Nozawa, Y. Hosokoshi, M. Ishikawa, M. Takahashi, M. Kinoshita, *Chem. Phys. Lett.* **1991**, *186*, 401; b) Y. Nakazawa, M. Tamura, N. Shirakawa, D. Shiomi, M. Takahashi, M. Kinoshita, M. Ishikawa, *Phys. Rev.* **1992**, *B46*, 8906; c) T. Sugawara, M. M. Matsushita, A. Izuoka, N. Wada, N. Takeda, M. Ishikawa, *J. Chem. Soc. Chem. Commun.* **1994**, *1723*. d) M. Deumal, J. Cirujeda, J. Veciana, M. Kinoshita, Y. Hosokoshi, J. Novoa, *Chem. Phys. Lett.* **1997**, *265*, 190.

Received: June 2, 1998
Revised version: January 4, 1999 [F1182]

0947-6539/99/0505-1480 $ 17.50+.50/0